

## WATER CONTENT TRENDS IN LOW-MASS MULTIPLANETARY SYSTEMS

L. Acu a<sup>1,2</sup>, M. Deleuil<sup>2,3</sup>, O. Mousis<sup>2,3</sup>, T. A. Lopez<sup>2</sup>, T. Morel<sup>4</sup>, A. Aguchine<sup>2,5</sup>, E. Marcq<sup>6</sup> and A. Santerne<sup>2</sup>

**Abstract.** Both rocky super-Earths and volatile-rich sub-Neptunes have been found simultaneously in multi-planetary systems, suggesting that these systems are appropriate to study different composition and formation pathways within the same environment. To estimate their composition, we present an interior structure model that includes self-consistently an atmosphere in radiative-convective equilibrium. We use our interior-atmosphere model within a Bayesian adaptive Markov Chain Monte Carlo (MCMC) for the detailed analysis of individual planets, allowing to estimate the uncertainties of the compositional parameters, core mass fraction and water mass fraction, given the error bars of the observed mass and radius. In this talk, I will present the development of this compositional model for super-Earths and sub-Neptunes, as well as its application to different planetary systems. I will focus in particular on the homogeneous analysis of a sample of multi-planetary systems hosting 5 or more exoplanets. Their composition gives us clues about their possible formation site in the protoplanetary disk and their formation mechanisms, including atmospheric escape. I will also discuss the uncertainties and degeneracies interior models face when estimating the volatile content of low-mass planets, and how JWST and future telescopes can help narrow down their possible compositions.

Keywords: Planetary interiors, Planetary composition, Numerical methods

### 1 Introduction

Low-mass exoplanets ( $M < 20 M_{\oplus}$ ) present two sub-populations based on their radius: super-Earths and rocky Earth-sized planets ( $R \sim 1.3 R_{\oplus}$ ) and sub-Neptunes ( $R \sim 2.4 R_{\oplus}$ ). The composition of the former sub-population is dominated by Fe and silicates that are found in the core and mantle, respectively, whereas sub-Neptunes are mostly composed by volatiles (Fulton et al. 2017; Fulton & Petigura 2018). It is still an open question whether super-Earths present a thin, low-mass atmosphere, or a bare rocky surface. If a thin atmosphere exists, the atmospheric composition would not present  $H_2$ , but high molecular weight species such as  $H_2O$ ,  $CO_2$ ,  $O_2$  or  $N_2$ . In contrast, sub-Neptunes can be constituted by: 1) a rocky core underneath a supercritical or ice water layer (depending on the irradiation of the planet), 2) a H-dominated envelope, or 3) an intermediate atmospheric composition with both  $H_2O$  and  $H_2$  in significant concentrations.

The first assessment of the composition of a planet is carried out by comparing its mass and radius to interior models. These models generate mass-radius relations that estimate the radius of a planet given its mass for a fixed composition. The mass and radius of a planet can be matched with mass-radius relations at different compositions, showing that there are degeneracies between the Fe and volatile content for super-Earths, and between the atmospheric mass and metallicity for sub-Neptunes. Therefore, atmospheric characterization observations are necessary to break these degeneracies in planetary interiors. Nonetheless, there are several instances where the characterization of the atmosphere may be difficult. This is the case of planets that present

<sup>1</sup> Max-Planck Institut f ur Astronomie, K onigstuhl 17, 69117 Heidelberg, Germany. e-mail: acuna@mpia.de

<sup>2</sup> Aix-Marseille Universit , CNRS, CNES, Institut Origines, LAM, Marseille, France.

<sup>3</sup> Institut universitaire de France (IUF), France

<sup>4</sup> Space sciences, Technologies and Astrophysics Research (STAR) Institute, Universit  de Li ge, Quartier Agora, All e du 6 Ao t 19c, B t. B5C, 4000 Li ge, Belgium

<sup>5</sup> Department of Astronomy and Astrophysics, University of California, 1156 High St, Santa Cruz, CA 95064, USA

<sup>6</sup> LATMOS/CNRS/Sorbonne Universit /UVSQ, 11 boulevard d'Alembert, Guyancourt, 78280, France

clouds and hazes, and whose transmission spectrum is flat (i.e. GJ1214 b, Gao et al. 2023), and planets whose stellar host is active and presents stellar contamination (TRAPPIST-1, see Ducrot et al. 2018; Zhang et al. 2018). In addition, the transmission spectrum may present a degeneracy to explain a particular spectral feature between two different opacity sources, making it difficult to set constraints on their abundances (see the case of water and methane in K2-18 b, Tsiraras et al. 2019; Bézard et al. 2022). Therefore, in these cases, interior models may be combined with atmospheric models to support the characterization of the bulk composition. In this talk, I will present an interior-atmospheric model applicable to terrestrial and water-rich compositions for low-mass planets (see Sect. 2). We apply this model to a sample of high multiplicity systems ( $n_{planets} \geq 5$ ) and connect their composition to different planet formation processes (see Sect. 3). We conclude with our final remarks on the water content of super-Earths and sub-Neptunes (see Sect. 4).

## 2 Model

### 2.1 Interior

Our one-dimensional (1D) interior structure model is differentiated in three layers: a hydrosphere, a silicate-rich mantle, and a Fe-rich core. Along the 1D grid that represents the radius, we solve a set of differential equations to obtain the planetary profiles: pressure, temperature, gravity, density and enclosed mass. These are computed by assuming hydrostatic equilibrium, an adiabatic profile, the gravitational force produced by the enclosed mass, the equation of state (EOS), and conservation of mass, respectively. The total mass of the planet, as well as the mass fraction of the core (CMF), and the water mass fraction (WMF) are the input parameters. The boundary conditions include the pressure and temperature at the top interface of the outermost layer,  $P_{base}$  and  $T_{base}$ . The model iterates the planetary profiles until these and the masses of all layers converge to constant values, obtaining as output the total planetary radius (Brugger et al. 2016, 2017).

For highly irradiated planets, the surface conditions cannot maintain water in its liquid or ice phases. Instead, the expected phases of water at high temperatures are vapour and supercritical. Therefore, we use an EOS that is valid within the supercritical and plasma pressure and temperature range. Furthermore, we couple an atmospheric model with the interior to determine self-consistently its boundary temperature since the density of the supercritical water layer is sensitive to the temperature. For water-rich planets, the supercritical envelope is massive enough to sustain high pressures at the interface between the hydrosphere and the mantle. For these volatile-rich planets, the interior and the atmosphere are coupled at a fixed pressure level of 300 bars because this is close enough to 1) the critical point of water, to prevent unphysical behaviour of the EOS, and 2) the maximum limit for which the opacity data used in atmospheric models is available. For planets whose atmospheric surface pressure is less than 300 bar, we couple the interior and the atmosphere at the physical planetary surface, which is the interface between the silicate mantle and the atmosphere. Further details on the coupling scheme between the interior and the atmospheric models can be found in Acuña et al. (2021).

### 2.2 Atmosphere

To obtain self-consistently the temperature at the base of the atmosphere, we use RADCONV1D, a 1D k-correlated atmospheric model that calculates low-resolution emission and reflection spectra of water-dominated atmospheres (Marcq et al. 2017; Pluriel et al. 2019). The thermal structure of the atmosphere is prescribed as a near-surface convective layer that is unsaturated, which means that the temperature gradient follows a dry adiabat. For the atmospheric layers where the pressure is below the saturation pressure of water, vapor condenses to form water clouds. Consequently, in the convective layer immediately above the near-surface unsaturated one, the temperature is computed with a wet adiabat. The topmost layer in the atmosphere is a radiative isothermal mesosphere.

The atmospheric model takes as input the surface pressure and temperature, and the enclosed mass and radius between the center and the surface of the planet. For our calculations, we consider a water-dominated envelope with 99% vapor and 1% CO<sub>2</sub>. Once the atmospheric structure is calculated, we solve the radiative transfer equation with DISORT (Stamnes et al. 2017) to obtain the outward emission at the top of the atmosphere and the reflection spectrum. Then these are integrated over wavelength to compute the outgoing longwave radiation (OLR) and the Bond albedo,  $A_B$  (Pluriel et al. 2019). With these two parameters, we solve with a root-finding method for the surface temperature at which the OLR and the absorbed flux are equal. The absorbed flux is calculated as  $F_{abs} = \sigma T_{eq}^4$ , where  $\sigma$  is the Stefan-Boltzmann constant. The equilibrium

temperature is defined as  $T_{eq} = (1 - A_B)^{0.25} (R_\star/2a_d)^{0.5} T_\star$ , where  $R_\star$  and  $T_\star$  are the stellar radius and effective temperature, and  $a_d$  is the planetary semi-major axis.

### 3 Multiplanetary systems

We combine our forward interior structure model with a Markov chain Monte-Carlo (MCMC) and apply it to a sample of multiplanetary systems. Multiplanetary systems are environments suitable to explore the compositional diversity of low-mass planets, as well as their formation and evolution. The aim of this work is to perform a homogeneous analysis, in other words, use the same interior-atmosphere model under similar assumptions, to obtain the WMF and CMF of planets in different systems, and compare their compositions. The MCMC retrieval on mass and radius data allows us to obtain the posterior distribution functions of the CMF and WMF, which determines the mean and uncertainties of these two compositional parameters.

We select multiplanetary systems that host low-mass planets only ( $M < 20 M_\oplus$ ), with 5 or more planets. Our final sample consists of 6 multiplanetary systems, including TRAPPIST-1 (Agol et al. 2021; Acuña et al. 2021), K2-138 (Lopez et al. 2019), TOI-178 (Leleu et al. 2021), Kepler-11, Kepler-102 and Kepler-80.

From our interior analysis, we find that TRAPPIST-1 b and c most likely have no atmosphere. For planet b, this is in agreement with JWST's emission photometry data (Greene et al. 2023; Ih et al. 2023). For planet c, the emission flux at 15  $\mu\text{m}$  discards a thick CO<sub>2</sub> atmosphere, although it is still compatible with a thin atmosphere of other compositions, such as N<sub>2</sub>, O<sub>2</sub> and water vapor (Zieba et al. 2023). With our interior structure retrieval, we constrain the maximum 1 $\sigma$  surface pressure for TRAPPIST-1 c as  $P_{surf,max} = 80$  bar (Acuña et al. 2023). For TRAPPIST-1 d, a liquid water envelope is unlikely based on the surface temperature estimated by 1D radiative-convective and climate models. Nonetheless, water could still be present in the form of vapor mixed in a CO<sub>2</sub>-dominated envelope. We calculate mass-radius relations for this scenario in planet d, and find that the density of TRAPPIST-1 d would be compatible with a maximum surface pressure of 300 bars. This is also in agreement with the maximum surface pressure that can be outgassed by a magma ocean in small planets (Baumeister et al. 2023). Furthermore, TRAPPIST-1 e to h present a trend where the WMF grows as the distance from the star increases. The system K2-138 also presents this trend in the WMF. The rest of the planetary systems show a diversity on their WMF vs incident irradiation trend (see Fig. 1). Nonetheless, all multiplanetary systems have in common that: 1) the inner planets are dry, and 2) the volatile-rich planets (water or H/He envelopes) are found in the outer part of the system. This can be explained by formation of the volatile-rich, outer planets in the vicinity of the water ice line, where volatile are more abundant for accretion than in the inner part of the protoplanetary disk. Many of these systems present mean motion resonances, which is indicative of later inward migration to their current location.

Moreover, some of the planets in our sample are not compatible with water envelopes in hydrostatic equilibrium because their observed radius is larger than the radius of a pure water planet by more than 1 $\sigma$ . For these planets, we estimate Jeans and XUV atmospheric escape in the energy-limited approximation (Aguichine et al. 2021) to discern whether their envelopes are H/He-dominated and in equilibrium, or are undergoing atmospheric escape. K2-138 g, TOI-178 g, and Kepler-11 c to e are candidates to having H/He-rich envelopes without atmospheric escape, whereas TOI-178 d, Kepler-11 f, Kepler-102 f and Kepler-80 g have lost more than 0.1  $M_\oplus$  due to Jeans escape. This escape mechanism is caused by the low surface gravity due to a small planetary core.

Regarding the Fe content of the planets in multiplanetary systems, planets whose CMF is larger than that of Mercury, are found in the innermost part of their respective systems. Collisions, mantle stripping and mantle evaporation have been proposed to explain their high Fe content. In addition, formation in the vicinity of refractory lines, particularly Fe and Si, explains how these planets could have accreted material that is rich in Fe (Aguichine et al. 2020).

### 4 Conclusions

We perform an interior structure, homogeneous analysis of the composition of planets hosted in multiplanetary systems. Our retrieval on mass and radius data provides the posterior distributions functions of the water and Fe content, allowing us to compare the composition of planets within a system. From our analysis, we find that: 1) multiplanetary systems show a clear separation between the inner, dry planets, and the outer, volatile-rich planets, 2) our CMF and WMF can be used to constrain formation site with respect to ice and refractory lines, as well as evolution mechanisms, such as Jeans escape. The typical water content of the inner,

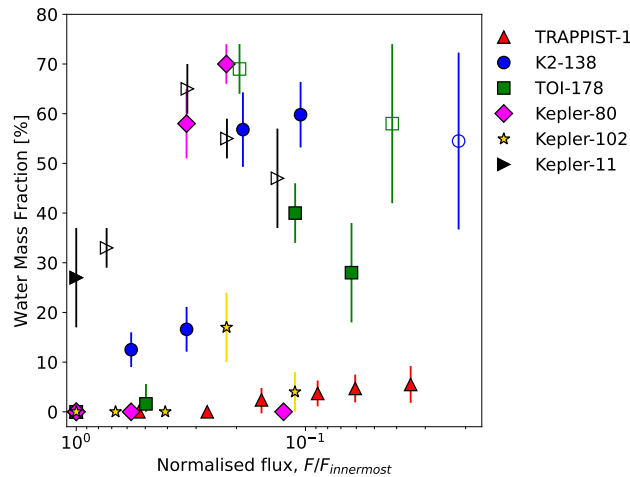


**Fig. 1.** Water mass fraction trends in multiplanetary systems as a function of the stellar incident flux. The fluxes are normalised to the flux of the innermost planet in their respective system.

dry planets is  $WMF < 5\%$ . Moderately volatile-rich sub-Neptunes have  $WMF = 10$  to  $25\%$ . Sub-Neptunes whose water content is estimated as  $WMF > 30\%$  with our interior model are good candidates for planets with H/He envelopes. Atmospheric characterization data is necessary to break the degeneracy between water and H/He for these sub-Neptunes.

M.D. and O.M. acknowledge support from CNES. This research has made use of the services of the ESO Science Archive Facility, the AAVSO Photometric All-Sky Survey (APASS), the Two Micron All Sky Survey, the Wide-field Infrared Survey Explorer, the K2 mission, the Exoplanet Follow-up Observation Program website, NASA's Astrophysics Data System Bibliographic Services, ESA's mission Gaia, the VizieR catalogue access tool.

## References

- Acuña, L., Deleuil, M., & Mousis, O. 2023, *A&A*, 677, A14  
 Acuña, L., Deleuil, M., Mousis, O., et al. 2021, *A&A*, 647, A53  
 Agol, E., Dorn, C., Grimm, S. L., et al. 2021, *PSJ*, 2, 1  
 Aguichine, A., Mousis, O., Deleuil, M., & Marcq, E. 2021, *ApJ*, 914, 84  
 Aguichine, A., Mousis, O., Devouard, B., & Ronnet, T. 2020, *ApJ*, 901, 97  
 Baumeister, P., Tosi, N., Brachmann, C., Grenfell, J. L., & Noack, L. 2023, *A&A*, 675, A122  
 Bézard, B., Charnay, B., & Blain, D. 2022, *Nature Astronomy*, 6, 537  
 Brugger, B., Mousis, O., Deleuil, M., & Deschamps, F. 2017, *ApJ*, 850, 93  
 Brugger, B., Mousis, O., Deleuil, M., & Lunine, J. I. 2016, *ApJ*, 831, L16  
 Ducrot, E., Sestovic, M., Morris, B. M., et al. 2018, *AJ*, 156, 218  
 Fulton, B. J. & Petigura, E. A. 2018, *AJ*, 156, 264  
 Fulton, B. J., Petigura, E. A., Howard, A. W., et al. 2017, *AJ*, 154, 109  
 Gao, P., Piette, A. A. A., Steinrueck, M. E., et al. 2023, *ApJ*, 951, 96  
 Greene, T. P., Bell, T. J., Ducrot, E., et al. 2023, *Nature*, 618, 39  
 Ih, J., Kempton, E. M. R., Whittaker, E. A., & Lessard, M. 2023, *ApJ*, 952, L4  
 Leleu, A., Alibert, Y., Hara, N. C., et al. 2021, *A&A*, 649, A26  
 Lopez, T. A., Barros, S. C. C., Santerne, A., et al. 2019, *A&A*, 631, A90  
 Marcq, E., Salvador, A., Massol, H., & Davaille, A. 2017, *Journal of Geophysical Research (Planets)*, 122, 1539  
 Pluriel, W., Marcq, E., & Turbet, M. 2019, *Icarus*, 317, 583  
 Stammes, K., Tsay, S. C., Jayaweera, K., et al. 2017, DISORT: DIScrete Ordinate Radiative Transfer, Astrophysics Source Code Library, record ascl:1708.006  
 Tsiaras, A., Waldmann, I. P., Tinetti, G., Tennyson, J., & Yurchenko, S. N. 2019, *Nature Astronomy*, 3, 1156  
 Zhang, Z., Zhou, Y., Rackham, B. V., & Apai, D. 2018, *AJ*, 156, 178  
 Zieba, S., Kreidberg, L., Ducrot, E., et al. 2023, *Nature*, 620, 746